

Article

Phytochemical-Assisted Green Synthesis of Nickel Oxide Nanoparticles for Application as Electrocatalysts in Oxygen Evolution Reaction

Vidhya Selvanathan ¹, M. Shahinuzzaman ^{2,*} , Shankary Selvanathan ³, Dilip Kumar Sarkar ¹, Norah Algethami ⁴, Hend I. Alkhamash ⁵, Farah Hannan Anuar ⁶ , Zalita Zainuddin ⁷, Mohammad Aminuzzaman ^{8,9}, Huda Abdullah ¹⁰ and Md. Akhtaruzzaman ^{1,*} 

- ¹ Solar Energy Research Institute (SERI), Universiti Kebangsaan Malaysia (UKM), Bangi 43600, Selangor, Malaysia; vidhya@ukm.edu.my (V.S.); dilipks551@gmail.com (D.K.S.)
- ² School of Computer Science and Information Technology, Central University of Science and Technology, Dhaka 1216, Bangladesh
- ³ Department of Chemistry, Faculty of Science, University of Malaya, Kuala Lumpur 50603, Malaysia; shankaryselvanathan@gmail.com
- ⁴ Department of Physics, Faculty of Science, Taif University, Taif 21944, Saudi Arabia; n.alkthamy@tu.edu.sa
- ⁵ Department of Electrical Engineering, College of Engineering, Taif University, Taif 21944, Saudi Arabia; Khamash.h@tu.edu.sa
- ⁶ Department of Chemistry, Faculty of Science and Technology, Universiti Kebangsaan Malaysia (UKM), Bangi 43600, Selangor, Malaysia; farahhannan@ukm.edu.my
- ⁷ Department of Physics, Faculty of Science and Technology, Universiti Kebangsaan Malaysia (UKM), Bangi 43600, Selangor, Malaysia; zazai@ukm.edu.my
- ⁸ Department of Chemical Science, Faculty of Science, Universiti Tunku Abdul Rahman (UTAR), Perak Campus, Jalan Universiti, Bandar Barat, Kampar 31900, Perak, Malaysia; mohammoda@utar.edu.my
- ⁹ Centre for Photonics and Advanced Materials Research (CPAMR), Universiti Tunku Abdul Rahman (UTAR), Jalan Sungai Long, Bandar Sungai Long, Kajang 43000, Selangor, Malaysia
- ¹⁰ Department of Electrical, Electronic & Systems Engineering, Faculty of Engineering & Built Environment, Universiti Kebangsaan Malaysia (UKM), Bangi 43600, Selangor, Malaysia; huda.abdullah@ukm.edu.my
- * Correspondence: shahinchmiu@gmail.com (M.S.); akhtar@ukm.edu.my (M.A.); Tel.: +603-89118587 (M.S. & M.A.)



Citation: Selvanathan, V.; Shahinuzzaman, M.; Selvanathan, S.; Sarkar, D.K.; Algethami, N.; Alkhamash, H.I.; Anuar, F.H.; Zainuddin, Z.; Aminuzzaman, M.; Abdullah, H.; et al. Phytochemical-Assisted Green Synthesis of Nickel Oxide Nanoparticles for Application as Electrocatalysts in Oxygen Evolution Reaction. *Catalysts* **2021**, *11*, 1523. <https://doi.org/10.3390/catal11121523>

Academic Editors: Stéphanie Lambert and Julien Mahy

Received: 20 November 2021
Accepted: 11 December 2021
Published: 15 December 2021

Publisher's Note: MDPI stays neutral with regard to jurisdictional claims in published maps and institutional affiliations.



Copyright: © 2021 by the authors. Licensee MDPI, Basel, Switzerland. This article is an open access article distributed under the terms and conditions of the Creative Commons Attribution (CC BY) license (<https://creativecommons.org/licenses/by/4.0/>).

Abstract: Electrocatalytic water splitting is a promising solution to resolve the global energy crisis. Tuning the morphology and particle size is a crucial aspect in designing a highly efficient nanomaterials-based electrocatalyst for water splitting. Herein, green synthesis of nickel oxide nanoparticles using phytochemicals from three different sources was employed to synthesize nickel oxide nanoparticles (NiO_x NPs). Nickel (II) acetate tetrahydrate was reacted in presence of *aloe vera* leaves extract, papaya peel extract and dragon fruit peel extract, respectively, and the physicochemical properties of the biosynthesized NPs were compared to sodium hydroxide (NaOH)-mediated NiO_x. Based on the average particle size calculation from Scherrer's equation, using X-ray diffractograms and field-emission scanning electron microscope analysis revealed that all three biosynthesized NiO_x NPs have smaller particle size than that synthesized using the base. Aloe-vera-mediated NiO_x NPs exhibited the best electrocatalytic performance with an overpotential of 413 mV at 10 mA cm⁻² and a Tafel slope of 95 mV dec⁻¹. Electrochemical surface area (ECSA) measurement and electrochemical impedance spectroscopic analysis verified that the high surface area, efficient charge-transfer kinetics and higher conductivity of aloe-vera-mediated NiO_x NPs contribute to its low overpotential values.

Keywords: green synthesis; nickel oxide; nanoparticles; oxygen evolution reaction; electrocatalysts

1. Introduction

One of the greatest challenges of the technological era is the inflating global energy demand as electricity becomes a necessity in every facet of life. The non-renewable nature of fossil-fuel-based energy production has stimulated the pursuit of sustainable energy

sources such as solar and wind energy. To overcome the intermittency issues of these renewable energy sources, production of hydrogen fuel from electrocatalytic water splitting is considered a strategic approach. Under a standard environment, 1.23 V of thermodynamic potential is required to drive electrochemical water splitting [1]. Nonetheless, in practical conditions, the sluggish kinetics of oxygen evolution reaction (OER) mandates high overpotential to generate the required current density. Hence, most practical electrolyzers consume more than 1.23 V to drive the desired reaction.

Electrocatalysts are usually employed to attain satisfactory water-splitting efficiency, but by far best electrocatalytic performance was demonstrated by noble-metal-based materials (e.g., RuO₂ and IrO₂). The high cost and low abundance of noble metals are not conducive for large-scale water-splitting applications. Therefore, non-precious transition metal oxides and hydroxides were explored as alternative electrocatalysts. Nickel oxide (NiO_x) is one such promising material for electrocatalytic water splitting due to its high electron transport capacity, good chemical stability and facile method of synthesis. Particularly, in the case of NiO_x NPs, the synthetic route adapted influences the electrical and structural properties of the material.

Traditionally, metal oxide nanoparticles are synthesized using a strong base as a reducing agent, followed by reaction with a capping agent or reducing agent. Sometimes, additional organic solvents are required to dissolve these capping agents. Alternatively, a green synthesis approach can be utilized to reduce the usage of unnecessary toxic chemicals [2]. In green synthesis, primary and secondary metabolites of plants are used to aid the synthesis of metal oxide nanoparticles [3]. These metabolites form a coating layer or stabilizing layer on the surface of the metal oxide nanoparticles and prevent intensive aggregation, thus yielding well-defined morphologies and tunable particle size [4]. The choice of plant species and its respective parts play an important role in determining the morphology and particle size of the NPs as they contain distinct phytochemical profiles [5].

One of the major advantages of chemical capping agents is the tunability of the species to yield nanoparticles with different particle size and morphology. For example, in the case of synthetic-polymers-based capping agents, factors such as the nature of polymer (functional group, branching), molecular weight and concentration were found to affect its function as a stabilizer [6]. However, in the context of green synthesis, much work is dedicated to exploring the effect of using a single plant extract formulation. Since each plant species comes with its unique cocktail of phytochemicals, it is useful to compare the effect of using different plant extracts on the overall size and morphology of the nanoparticles. Thus, in this study we have explored three different plant extracts, namely, *aloe vera* leaves extract, papaya fruit peel extract and dragon fruit peel extract, as capping agents for NiO_x NPs.

Aloe vera gel contains mostly water and polysaccharides, such as pectins, cellulose, hemicellulose, glucomannan and acemannan [7,8]. In addition to that, the aloe latex is made up of hydroxyanthracenic derivatives and anthraquinone glycosides, along with emodin. Papaya peel is rich in a variety of vitamins including β-carotene, vitamin B (thiamine, riboflavin, niacin and folate), vitamin C and vitamin E [9]. On the other hand, dragon fruit peel is reported to contain wide compositions of antioxidants such as betasianin, flavonoids, phenols, terpenoids, thiamine, niacin, pyridoxine and cobalamin [10]. The effect of these different phytochemical compositions of extracts on the structural and morphological properties of the NiO_x NPs and, consequently, their electrocatalytic activities for OER were studied and reported in detail.

2. Results and Discussion

2.1. Structural Properties

Figure 1 shows the structural properties of the synthesized NiO_x nanoparticles using different extracts after calcination at 300 °C and 600 °C. As shown in the diffractograms, all the samples exhibited diffraction peaks at 2θ values of 37.2, 43.2, 62.8, 75.4 and 79.4° attributed to (101), (012), (104), (113) and (006) crystal planes of cubic NiO_x [11,12]. These

peaks were in agreement with the standard JCPDS card no. 00-004-1159. Significant differences in the peak intensities were evident between samples calcined at 300 °C and 600 °C. At lower calcination temperature, the presence of organic residues from the plant extract used during NiO_x synthesis reduced the crystallinity of the nanoparticles. Upon calcination at 600 °C, high purity NiO_x nanoparticles were produced, leading to sharp and intense XRD peaks.

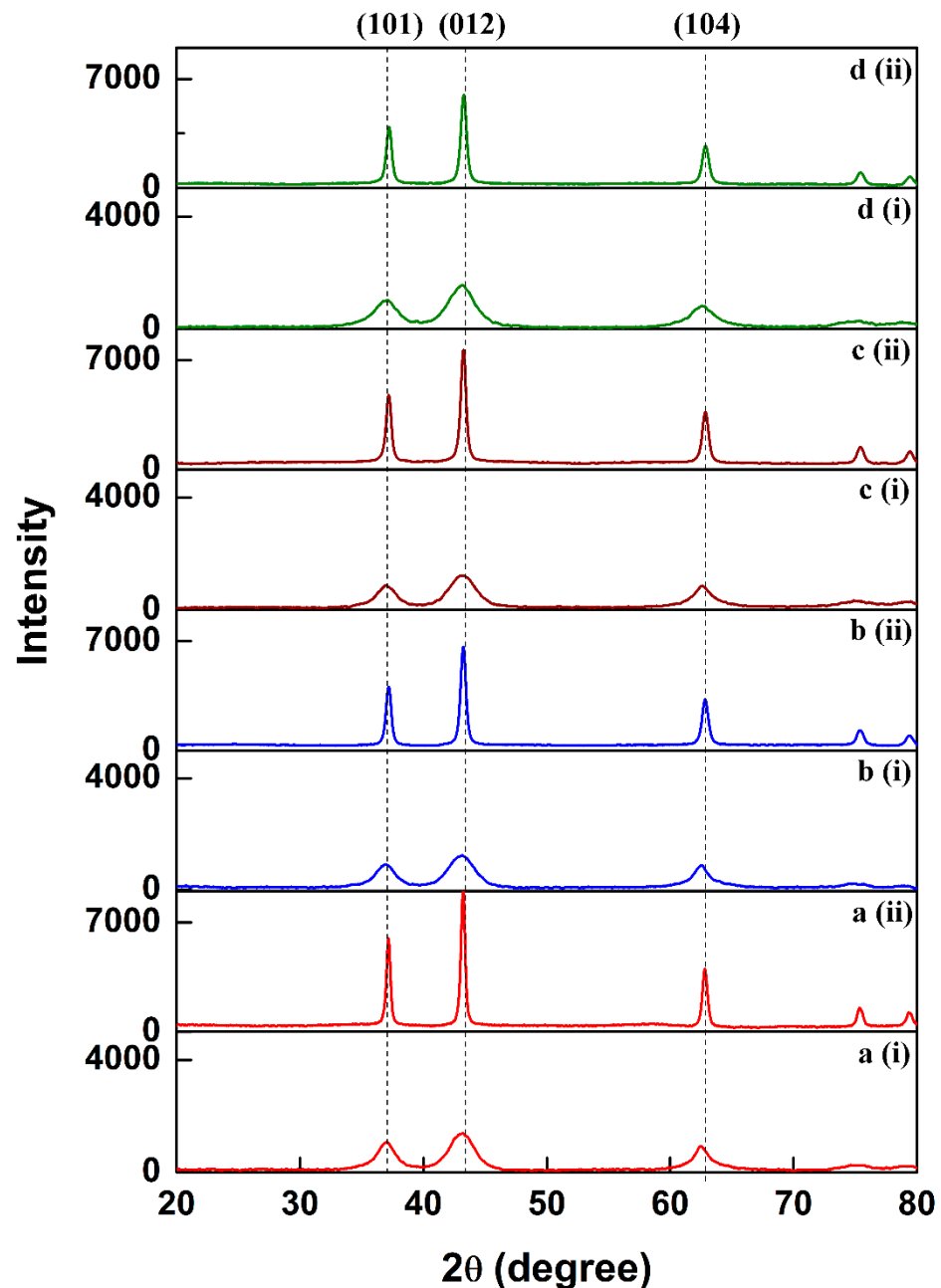


Figure 1. X-ray diffractogram of (a) NaOH-, (b) aloe-vera-, (c) dragon-fruit- and (d) papaya-extract-mediated NiO_x nanoparticles calcined at (i) 300 °C and (ii) 600 °C.

The average crystal sizes (D) were calculated based on the width of the peak due to the (200) planes by using the Scherrer's formula [13]:

$$D = \frac{0.94\lambda}{\beta \cos\theta} \quad (1)$$

From Table 1, it could be seen that the average crystallite size of the nanoparticles synthesized with only NaOH was 15.9 nm, whereas *aloe vera*, papaya and dragon fruit extracts was 11.5 nm, 8.1 nm and 10.2 nm, respectively. The reduced crystallite size of NiO_x nanoparticles synthesized in presence of plant extracts emphasizes the role of phytochemicals that are able to chelate with metal ions, thus acting as stabilizers or capping agents. Figure 2 illustrates the plausible mechanism for formation of NiO_x nanoparticles in this study. Upon dissolution, nickel acetate tetrahydrate dissociated to release Ni²⁺ ions which then combined with hydroxide ions from the base to form Ni(OH)₂. The continuous stirring under a heated environment enabled Ni(OH)₂ to thermally decompose into NiO nuclei [14]. The phytochemicals present in each plant extract served as capping ligands which formed interactions with the nanoparticles' surface, leading to steric hindrance and providing eventual stability to the nanocomposite. Hence, the presence of biomass-derived extracts controlled the particle size and minimized agglomeration of the nanoparticles.

Table 1. Particle size calculation based on Debye–Scherrer's equation.

Material	2θ	FWHM	βcosθ	Crystallite Size (nm)	Average Crystallite Size (nm)
NiO–NaOH	37.4	0.51	0.0085	16.3	15.9
	43.2	0.51	0.0083	16.8	
	62.8	0.63	0.0094	14.7	
NiO–Aloe	37.4	0.71	0.0117	11.8	11.5
	43.2	0.63	0.0101	13.6	
	62.8	1.03	0.0153	9.0	
NiO–Papaya	37.4	0.90	0.0149	9.3	10.2
	43.2	0.68	0.0109	12.6	
	62.8	1.08	0.0160	8.6	
NiO–Dragon	37.4	1.62	0.0269	5.2	8.1
	43.2	0.68	0.0109	12.6	
	62.8	1.45	0.0216	6.4	

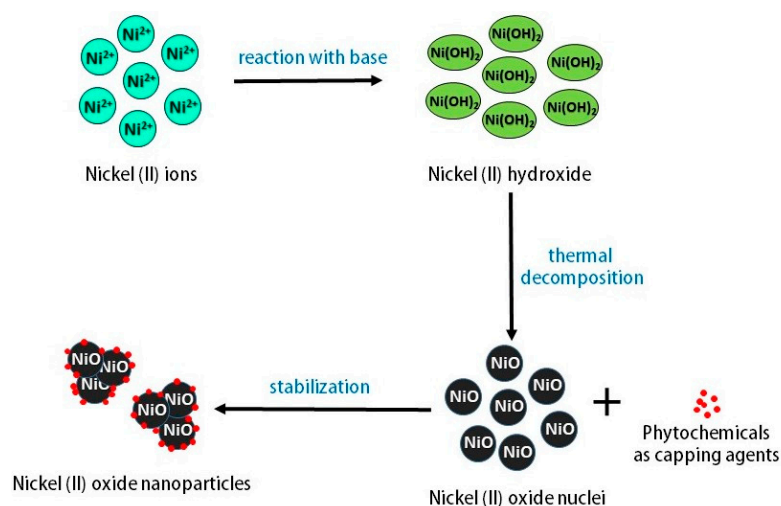


Figure 2. Plausible mechanism for green synthesis of NiO_x nanoparticles.

2.2. Morphological Properties

The morphological properties of the synthesized NiO_x nanoparticles are shown in Figure 3. From the images, it is clear that the NiO_x nanoparticles were spherical-shaped, densely packed and intercalated with each other. Dragon fruit and papaya-extract-mediated NiO_x NPs depict well-defined nanostructures with fewer intercalations. The particle size distribution for the NiO_x NPs synthesized without extract ranged between

40 and 60 nm, whereas plant-extract-mediated NiO_x NPs were between 20 and 30 nm in size. The trend in particle size coincided with the trend in crystallite size derived from the XRD analysis. For all the samples, the particle size revealed in morphological analysis was higher than average crystallite size estimated from XRD analysis, hence indicating that the single NiO_x particle is made up of few crystallites.

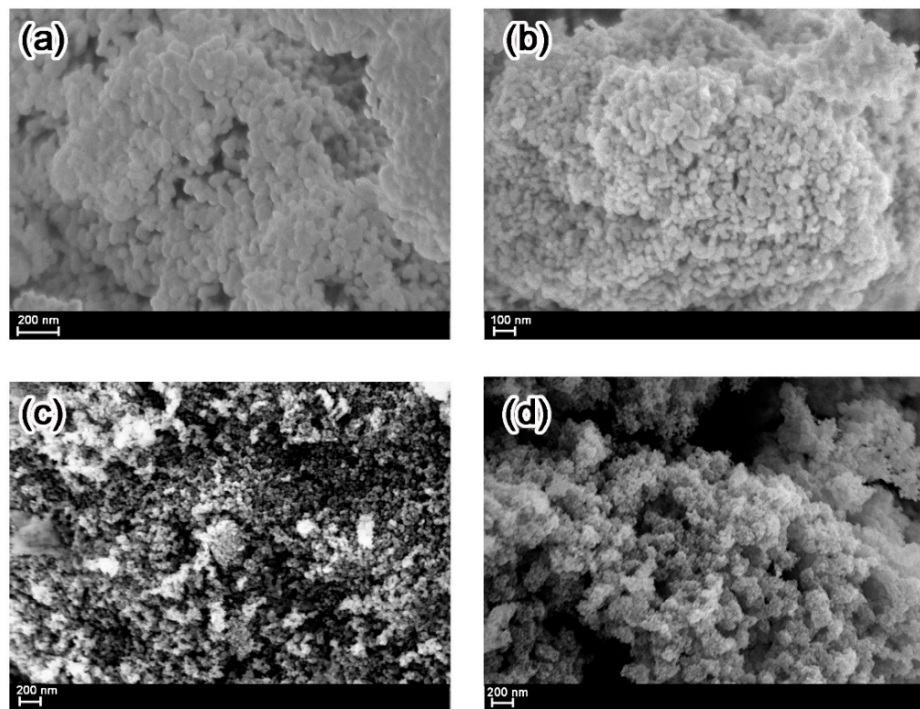


Figure 3. FESEM images of (a) NaOH-, (b) aloe-vera-, (c) dragon-fruit- and (d) papaya-extract-mediated NiO_x nanoparticles.

The elemental composition of the nanoparticles was verified from EDX analysis. As shown in Figure 4, the choice of plant extract influenced the composition of nickel and oxygen in the samples. NiO_x NPs synthesized using *aloe vera* were more oxygen deficient compared to papaya and dragon fruit. Aloe-vera-mediated nickel oxide also exhibited the highest amount of residual carbon, despite calcining the samples at 600 °C. It is deduced that this could be due to the more viscous nature of the *aloe vera* extract, which adheres to the surface of the nanoparticles during synthesis. The absence of residual carbon originating from the phytochemicals was evident in dragon-fruit- and papaya-extract-mediated NiO_x NPs, which could explain the occurrence of fewer intercalations, as shown in the FESEM images.

2.3. Optical Properties

The absorption spectrum of the NiO_x nanoparticles, as shown in Figure 5a, was recorded at room temperature within the range of 200–800 nm. There was a peak observed at around 300–350 nm for all synthesized nanopowders, which can be assigned to the exciton transitions [15]. The band gap energies were estimated by extrapolation using Tauc plots, and the energy curves are shown in Figure 5. It was seen that the band gap of NiO_x nanoparticle synthesis in different samples were ranging from 3.09 to 3.22 eV and the band gap was slightly increased for plant-extract-assisted synthesized nanoparticles. Particularly, the decrease in particle size, as well as the increase in band gap energy of the as-prepared nanoparticles, signified the size quantization effects [16]. When particle size reached the nanosized scale, the overlapping of adjacent energy levels minimized and, subsequently, the width of energy band widened [17,18].

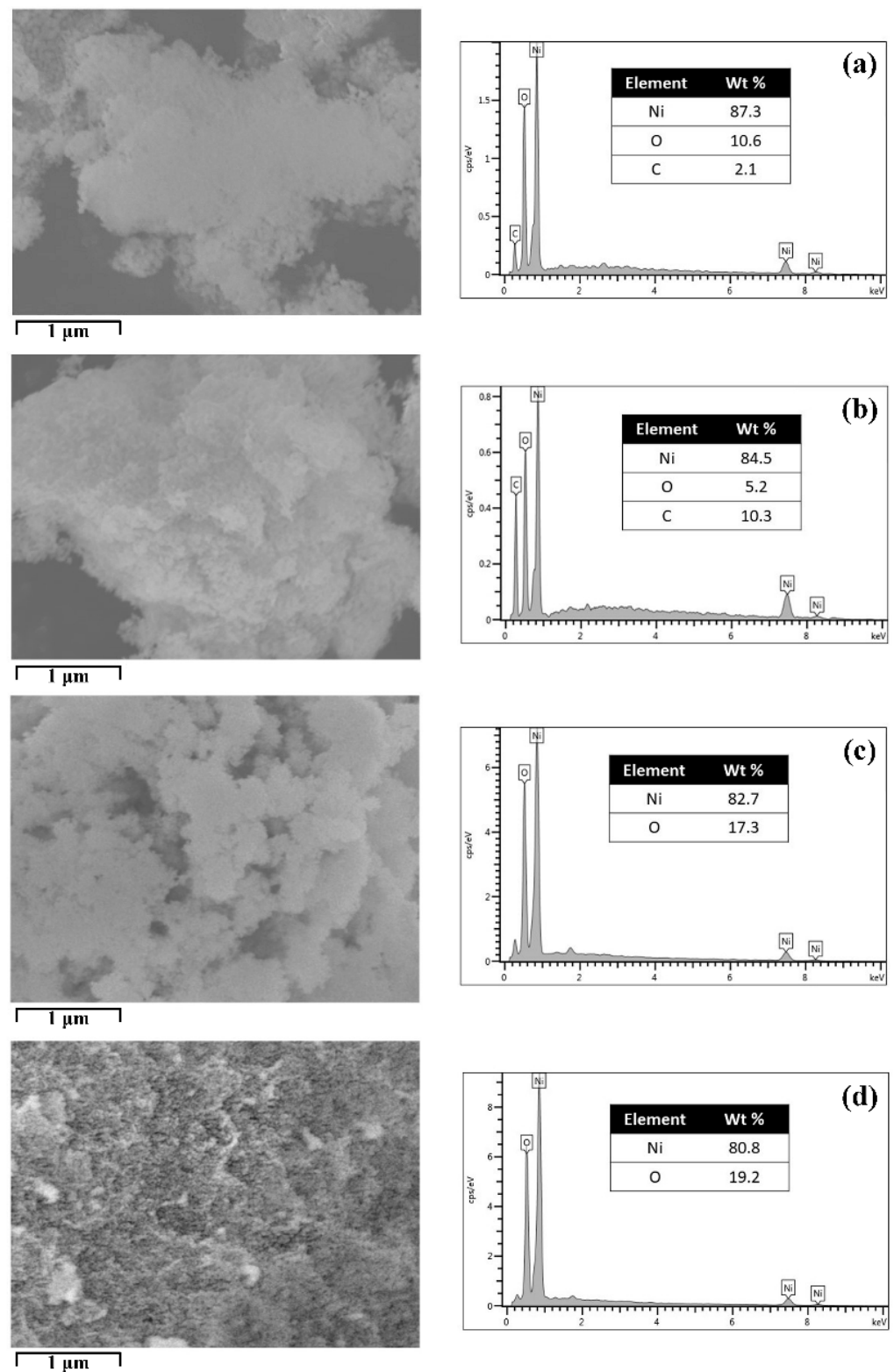


Figure 4. EDX spectrum of (a) NaOH-, (b) aloe-vera-, (c) dragon-fruit- and (d) papaya-extract-mediated NiO_x nanoparticles.

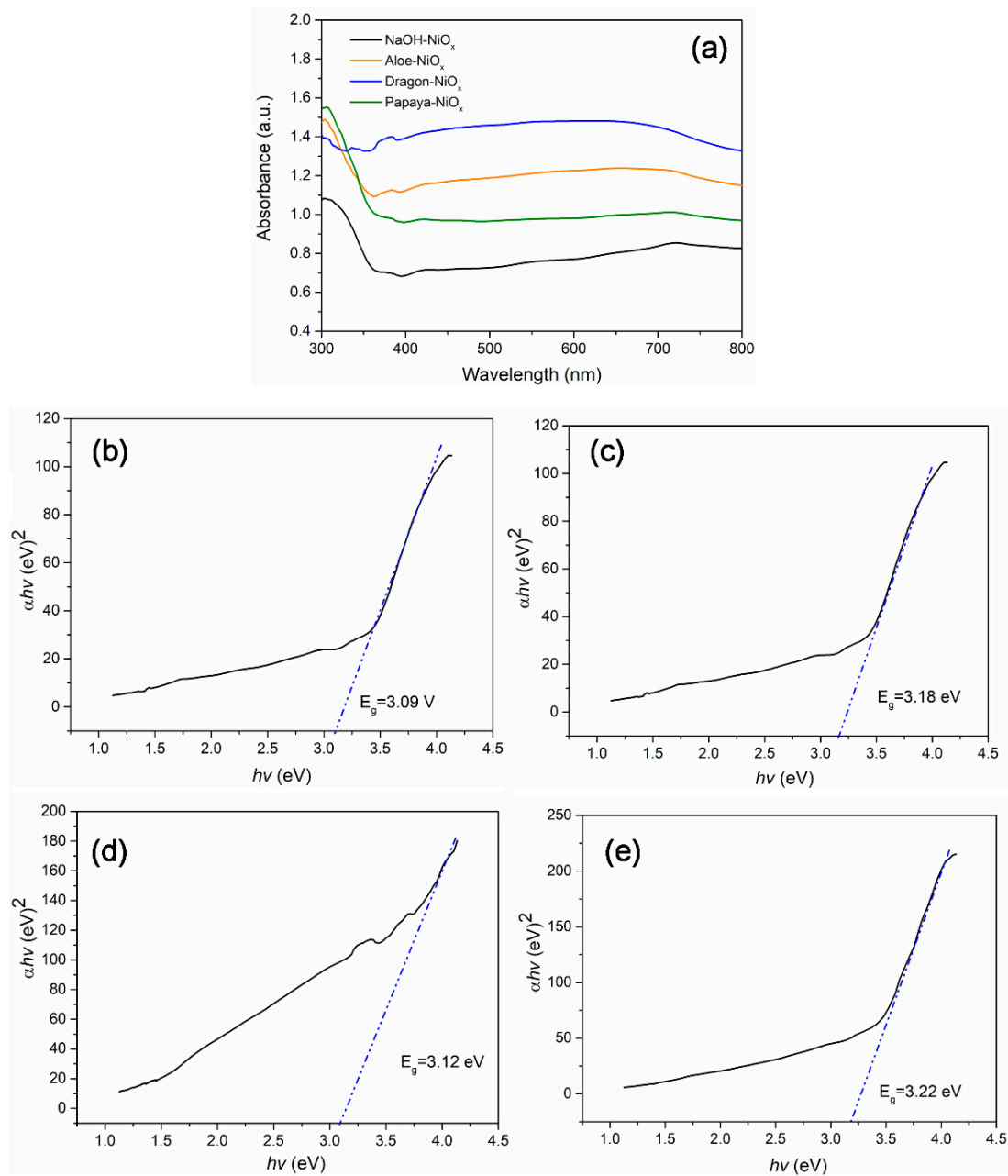


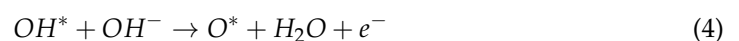
Figure 5. (a) UV-Vis absorption spectrum and the corresponding Tauc plot of (b) NaOH-, (c) aloe-vera-, (d) dragon-fruit- and (e) papaya-extract-mediated NiO_x nanoparticles.

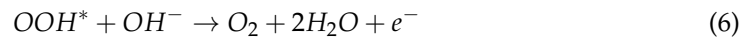
2.4. Electrocatalytic Properties for Oxygen Evolution Reaction (OER)

The electrocatalytic activity of the synthesized NiO_x NPs towards OER was explored by performing linear scanning voltammetry (LSV) in an aqueous solution of 1.0 M KOH. Generally, the oxygen evolution reaction in alkaline medium is represented as follows [19–21]:



The four-electron reaction mechanism can be described sequentially via the following equations:





where OH^* , O^* and OOH^* indicate the species adsorbed to the active site of the catalyst.

Based on the polarization curves shown in Figure 6a, to attain the current density of 10 mA cm^{-2} , aloe-vera- and papaya-extract-mediated NiO_x NPs exhibited the overpotential values of 416 mV and 433 mV, respectively, which are lower than NaOH-based NiO_x , which records 474 mV. Interestingly, dragon-fruit-extract-mediated NiO_x showed the overpotential of 501 mV, the highest overpotential compared to the previous three samples. As listed in Table 2, the onset potential, which indicates the voltage at which current begins to rise, was lowest for aloe-vera-mediated NPs and highest for dragon fruit.

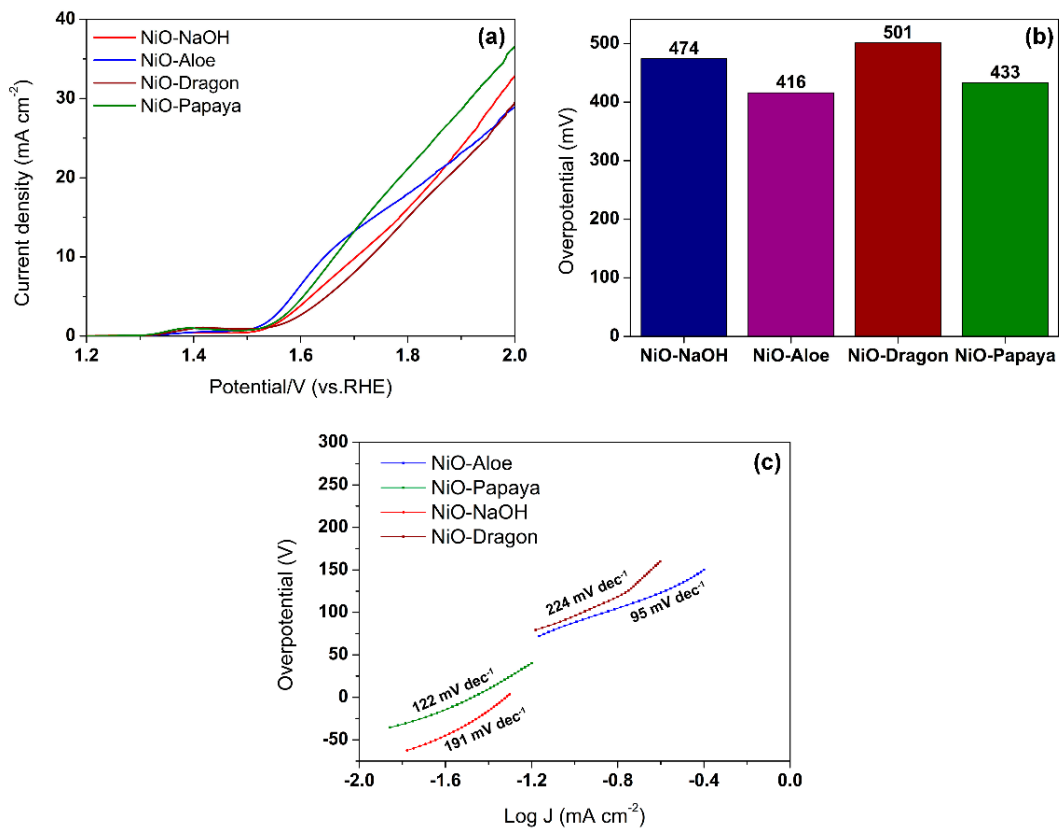
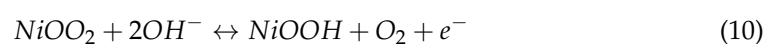
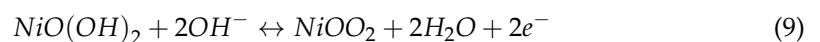
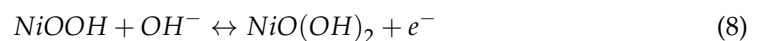
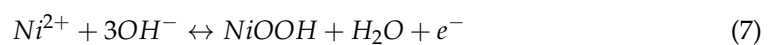


Figure 6. (a) Polarization curve by linear sweep voltammetry, (b) overpotential at 10 mA cm^{-2} and (c) Tafel plot.

Table 2. Electrocatalytic parameters of NiO_x nanoparticles.

Material	Onset Potential (V)	Overpotential at 10 mA cm^{-2} (mV)	Tafel Slope (mV dec^{-1})
NiO-NaOH	1.57	474	191
NiO-Aloe	1.54	416	95
NiO-Papaya	1.56	433	122
NiO-Dragon	1.59	501	224

The plausible reaction mechanism of NiO_x for OER is outlined as follows:



Throughout the electrocatalytic process, Ni^{2+} ions that can be present on surface of the NiO_x NPs will undergo oxidation to form Ni^{3+} ions which then aid to catalyze the oxidation of OH^- ions, leading to the formation of water [22].

To further comprehend the reaction kinetics of the nickel-oxide-based electrocatalysts, the Tafel plot was plotted (Figure 6c), and the linear section of Tafel slope was derived from the following equation:

$$\eta = b \log j + a \quad (11)$$

where η is the overpotential, b is the Tafel slope and j refers to current density. NaOH-, aloe-vera-, papaya- and dragon-fruit-mediated NiO_x recorded slope values of 191, 95, 122 and 224 mV/decade, respectively. The Tafel slope values indicate the rate-limiting step which is attributed to the reaction with first electron transfer. Thus, the lower Tafel slope value of aloe-vera-mediated NiO_x NPs translates to more efficient reaction kinetics for OER. One of the proposed explanations for the superior electrocatalytic performance of aloe-vera-mediated NiO_x NPs can be related to the relatively high oxygen deficiency in the samples, as evidenced by EDX measurements. The non-stoichiometric composition most likely led to the presence of surface defects, which have been found to enhance the electrocatalytic performance of metal oxides for OER [23,24].

Another key factor that governs the performance of electrocatalyst is the surface area available as active sites for catalytic activities. In OER, electrochemically active surface area (ECSA) is used as the parameter to assess the specific catalytic activity of an electrocatalyst, and it can be derived from electrochemical double-layer capacitance (C_{dl}). To calculate C_{dl} values, the samples were subjected to cyclic voltammetry (CV) at different scan rates in the non-Faradaic segment where the voltage was scanned from 1.46 to 1.56 V vs. RHE (Figure 7). The double-layer capacitance was then derived based on the gradient of linear plot of $\Delta J = (J_a - J_c)$ (where J_a and J_c are anodic and cathodic current density) at 1.52 V vs. RHE as a function of the scan rate [25]. The ECSA was then calculated from the double-layer capacitance based on the following equation:

$$ECSA = \frac{C_{dl}}{C_s} \quad (12)$$

where C_s is the specific capacitance which is equated to 0.040 mF cm^{-2} based on the conventional value for metal electrode in KOH solution. The roughness factor (R_f) can then be evaluated by dividing ECSA by the electrode area. Table 3 summarizes the ECSA and roughness factor for all the samples. Papaya-mediated NiO_x NPs exhibit the highest value of ECSA and R_f of 5.50 mFcm^{-2} and 1936, respectively, thus indicating that it has the highest catalytically active surface area. This could be the boosting factor that supports the low overpotential value recorded by papaya-mediated NiO_x NPs despite its high Tafel slope. The variation of active surface area of the electrocatalysts prepared using different plant extracts further emphasizes the role of phytochemicals in fine-tuning the morphology and size distribution of nanoparticles during the synthesis process.

Table 3. Electrochemical active surface area and double-layer capacitance of NiO_x nanoparticles.

Material	C_{dl} (mF cm ⁻²)	ECSA (cm ²)	R_f
NiO–NaOH	4.50	112.50	1584
NiO–Aloe	4.80	120.00	1690
NiO–Papaya	5.50	137.50	1936
NiO–Dragon	2.25	56.25	792

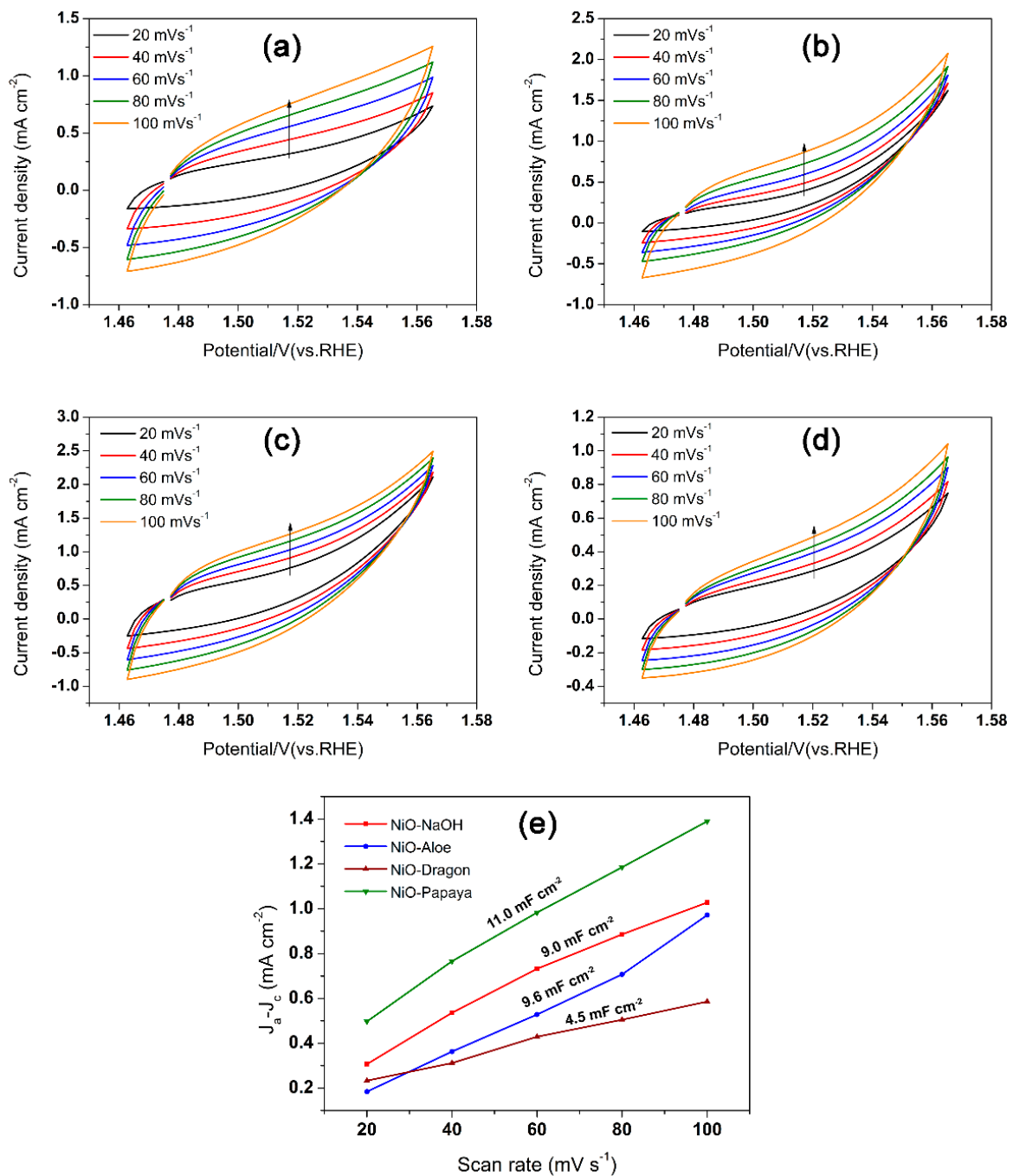


Figure 7. Cyclic voltammogram of (a) NaOH-, (b) aloe-vera-, (c) dragon-fruit- and (d) papaya-extract-mediated NiO_x nanoparticles and (e) linear plot between current density and scan rate.

Electrochemical impedance spectroscopy (EIS) is a powerful technique that allows us to obtain insights on electrode–electrolyte interface dynamics. The EIS measurements for all the samples were performed with a frequency range from 0.1 Hz to 100 kHz, and the resulting Nyquist plots comprising of semicircles are presented in Figure 8. The starting point of the semicircle signifies the internal resistance (also known as solution resistance (R_s)) of the catalyst, whereas the diameter of the semicircle denotes charge-transfer resistance between the electrode–electrolyte interfaces (R_{CT}) [26]. In terms of equivalent circuit, the depressed semicircle is represented by R_s connected in series to the

capacitor (Q_{DL}) and R_{CT} in a parallel arrangement, as shown in Figure 8. The following equation evaluates impedance values according to the described equivalent circuit [27]:

$$Z_{DSSC} = R_s + \frac{R_{CT}}{1 + (j\omega)^{n_{CT}} R_{CT} Q_{CT}} \quad (13)$$

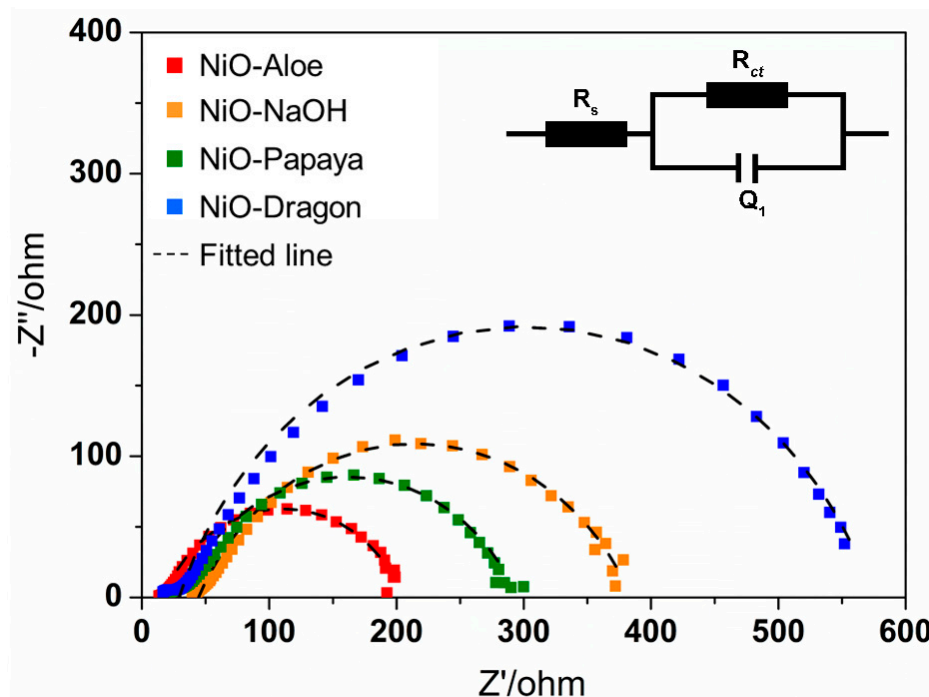


Figure 8. Nyquist plots from EIS analysis.

The equation was used to fit the Nyquist plots and the solution resistance, charge-transfer resistance and double-layer capacitance based on the equivalent circuit fitting are tabulated in Table 4. Typically, charge-transfer resistance (R_{CT}) is considered the most significant parameter as it dictates the extent of electronic transfers between the reactant and electrocatalyst surface. A lower R_{CT} value also indicates higher conductivity of the electrocatalyst material which favors electron mobility during the electrocatalytic reaction [28]. In this study, aloe-vera-mediated NiO_x NPs showed the lowest solution resistance and charge-transfer resistance. This can be attributed to better conductivity of the NiO_x NPs due to its higher oxygen deficiency compared to other green-synthesized nanoparticles. Therefore, it is evident that efficient charge-transfer kinetics and improved conductivity is one of the crucial factors for the higher electrocatalytic performance of aloe-vera-mediated NiO_x NPs compared to its dragon fruit and papaya counterparts.

Table 4. Equivalent circuit fitting parameters for the EIS analysis.

Material	R_s (Ω)	R_{CT} (Ω)	Q_{DL} (F)
NiO-NaOH	44.5	339.9	3.04×10^{-4}
NiO-Aloe	17.0	187.9	3.59×10^{-4}
NiO-Papaya	29.2	265.6	2.72×10^{-4}
NiO-Dragon	29.4	544.5	1.54×10^{-4}

To evaluate the stability of aloe-vera-mediated NiO_x NPs, chronoamperometry analysis was performed for 24 h at an overpotential of 415 mV. Within the first 2 h, it was observed that there was a gradual increase in current density. This is attributed to the activation of nickel oxide into nickel oxyhydroxide ($NiOOH$) during the initial part of

the analysis [22]. Higher conductivity of NiOOH compared to NiO rendered the gradual increase in current density. As the chronoamperometry was extended for 24 h, the current density remained stable without any significant decay.

The stability of the final product was further verified by subjecting the NiO_x-modified glassy carbon electrode to cyclic voltammetry (CV) analysis for 500 continuous cycles, which were carried out between 1.2 and 1.8 V at a scan rate of 100 mVs⁻¹. As shown in Figure 9, after 500 CV cycles, the overpotential of aloe-vera-mediated NiO_x NPs increased from 416 mV to 428 mV with a difference of only 0.12 mV at the current density of 10 mA cm⁻². This observation validates the high electrocatalytic stability of the green-synthesized nickel oxide nanoparticle for OER activity.

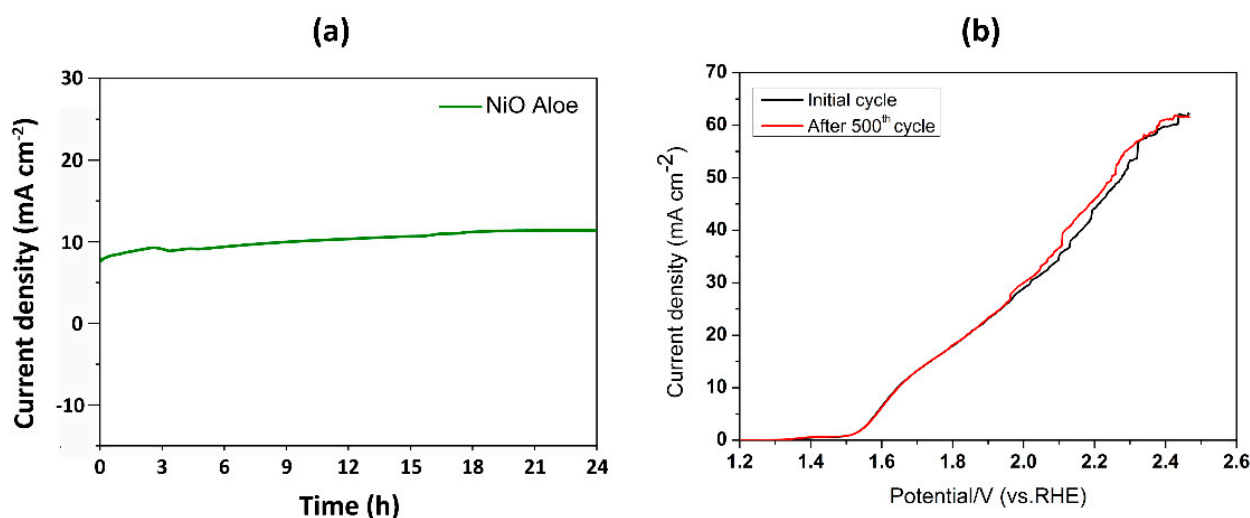


Figure 9. (a) Chronoamperometric stability tests at 1.65 V (vs the RHE) and (b) LSV curves obtained before and after 500 CV cycles of aloe-vera-mediated NiO_x NPs.

3. Materials and Methods

3.1. Chemicals

Nickel acetate tetrahydrate (Ni(CH₃COO)₂·4H₂O), NaOH and KOH were purchased from Sigma Aldrich, Hamburg, Germany. Deionized (DI) water was used to prepare all types of solution. All the other chemicals were of analytical reagent grade and used without any further purification.

3.2. Preparation of Plant Extract

The NiO_x nanoparticles were synthesized using various plant extracts such as *aloe vera* leaf extract, dragon fruit peel extract and papaya peel extract. NiO_x NPs without extract were also synthesized. Different plant samples were collected from the local market at Hentian Kajang, Selangor, Malaysia. In order to prepare the plant extract, at first, 50 g of different plant samples were washed with DI water, cut into small pieces and were taken in three different 500 mL glass beakers and 250 mL DI water was added to all the beakers. Then the mixtures were heated at 60–70 °C for 30 min with continuous stirring. After heating, the extracts were filtered with vacuum filter and the filtrates were collected in three different 500 mL reagent bottles.

3.3. Synthesis of NiO_x Nanoparticle

The NiO_x nanoparticles were synthesized using the green synthesis technique. In this technique, at first, 30 mL (1 M) nickel acetate solutions were heated in four different 250 mL glass beakers at 60–70 °C temperature with continuous stirring. Then, 30 mL DI water was added to the first beaker (without extract) and 30 mL of three different plant extracts to the other three beakers was added in the precursor solution with constant heating

(60–70 °C temperature) and stirring. Then, 1 M NaOH solution was added, dropwise, into the reaction mixture with vigorous stirring and heating for 2 h. After completion of the reaction, the mixtures were washed with DI water several times and filtered using Whatman 1 filter paper. Finally, the synthesized NPs were dried in an oven at 100 °C overnight, calcined at 300 °C and 600 °C for 6 h, powdered using mortar-pastel and stored in the glass vial for further analysis. Figure 10 represents the schematic view of green synthesis process of NiO_x NPs.

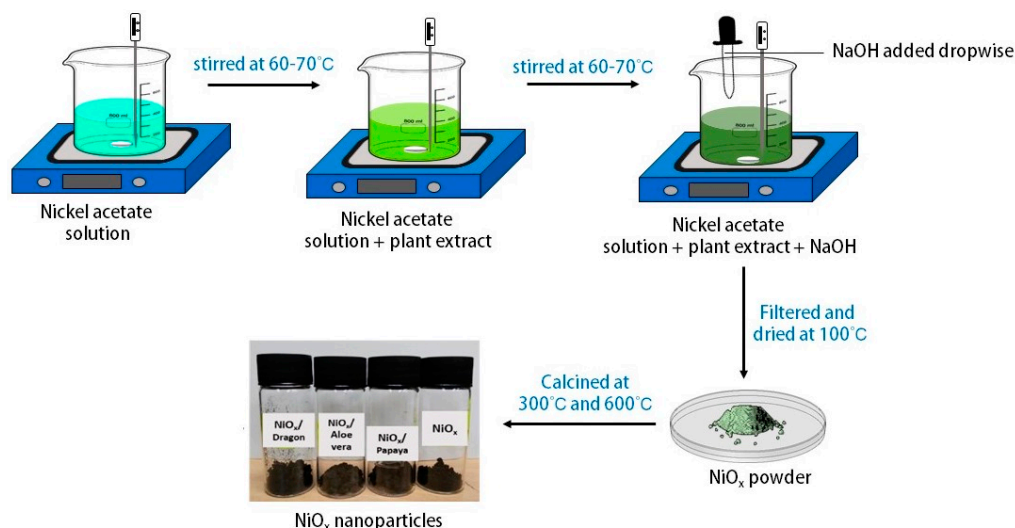


Figure 10. Reaction scheme for green synthesis process of NiO_x NPs.

3.4. Characterization of Materials

The morphological and structural properties of synthesized NiO_x nanoparticles were examined using various characterization techniques such as X-ray diffraction (XRD), absorption spectra (UV-Vis) and field-emission scanning electron microscopy (FESEM), along with energy dispersive X-ray (EDX). The XRD patterns were taken in the 2θ ranging from 10° to 80° using BRUKER aXS-D8 Advance Cu-Kα diffractometer (Bruker, MA, USA). The FESEM model LEO 1450 Vp was used for investigating the surface morphology, as well as grain size and growth of the NiO_x nanoparticles. The optoelectronic properties of the synthesized nanocatalyst, such as the optical transmittance, absorbance and optical band gap, were calculated using UV-Vis spectrometer Perkin Elmer Instruments Lambda35 (PerkinElmer, Waltham, MA, USA).

3.5. Electrochemical Characterization

Electrochemical characterization was performed using Metrohm Autolab workstation (Metrohm, Herisau, Switzerland) in a three-electrode setup in which platinum electrode and silver/silver chloride were used as the counter electrode and reference electrode, respectively. The NiO_x NPs were drop casted onto glassy carbon electrode with an active area of 0.07 cm² to function as the working electrode. A 5 mg amount of the NiO_x NPs was mixed with 250 μL ethanol, 250 μL deionized water and 50 μL of Nafion (5 wt%). The dispersion was sonicated for an hour and 10 μL of the dispersion was drop casted on top of the glassy carbon electrode surface followed by drying. Linear sweep voltammetry between 0 and 1 V with scan rate of 5 mV s⁻¹ was performed to evaluate the oxygen evolution reaction. The measured potential vs. Ag/AgCl was converted to a reversible hydrogen electrode (RHE) based on the following equation:

$$E_{RHE} = E_{Ag/AgCl} + 0.059 \text{ pH} + E_{Ag/AgCl}^0 \quad (14)$$

where $E_{Ag/AgCl}^0$ is 0.1976 V at 25 °C and $E_{Ag/AgCl}$ is measured potential vs. Ag/AgCl. The overpotential is calculated by measuring the difference between measured potential vs. RHE at current density of 10 mA cm⁻² and the standard value of 1.23 V.

4. Conclusions

Utilization of different plant extracts as capping agents affects the structural and morphological properties of NiO_x NPs. FESEM results show that NiO_x NPs synthesized without extract had a particle size between 40 and 60 nm, whereas plant-extract-mediated NiO_x were between 20 and 30 nm. The reduction in particle size upon introducing plant extracts was further supported by the shifting of the band gap to a higher value based on optical characterization. EDX analysis reveal that *aloe vera*, papaya and dragon fruit extract yielded NiO_x NPs with different oxygen and nitrogen stoichiometry. The deficiency of oxygen is higher in *aloe vera*-mediated NiO_x NPs, which might elevate its conductivity and thus lead to lower charge-transfer resistance in EIS analysis. ECSA calculation based on cyclic voltammetry indicated that the highest electrocatalytic surface area was possessed by papaya-extract-mediated NiO_x NPs, followed by *aloe vera* and dragon fruit extract. Overall, the best electrocatalytic performance is attributed to *aloe vera*-extract-mediated NiO_x NPs, which only required 433 mV overpotential to reach 10 mAcm⁻² with a Tafel slope of 95 mVdec⁻¹.

Author Contributions: Conceptualization, V.S, M.S. and S.S.; methodology, M.S., D.K.S. and M.A. (Mohammad Aminuzzaman); formal analysis, F.H.A. and Z.Z.; writing—original draft preparation, V.S. and S.S.; writing—review and editing, H.I.A. and N.A.; supervision, M.A. (Md. Akhtaruzzaman); project administration, H.A. and M.A. (Md. Akhtaruzzaman); funding acquisition, H.I.A. and N.A. All authors have read and agreed to the published version of the manuscript.

Funding: The authors are highly grateful to Universiti Kebangsaan Malaysia for supporting this study through the Modal Insan fellowship (RFA1). Authors also extend their appreciation to The University Researchers Supporting Project Number (TURSP-2020/264), Taif University, Taif, Saudi Arabia. Authors are thankful to Universiti Tunku Abdul Rahman (UTAR) providing necessary research facilities to carry out this research work successfully.

Data Availability Statement: Not applicable.

Acknowledgments: The authors are highly grateful to Universiti Kebangsaan Malaysia for supporting this study through the Modal Insan fellowship (RFA1). Authors also extend their appreciation to The University Researchers Supporting Project Number (TURSP-2020/264), Taif University, Taif, Saudi Arabia.

Conflicts of Interest: The authors declare no conflict of interest.

References

1. You, B.; Sun, Y. Innovative strategies for electrocatalytic water splitting. *Acc. Chem. Res.* **2018**, *51*, 1571–1580. [CrossRef]
2. Pal, G.; Rai, P.; Pandey, A. Chapter 1—Green synthesis of nanoparticles: A greener approach for a cleaner future. In *Green Synthesis, Characterization and Applications of Nanoparticles*; Shukla, A.K., Irvani, S., Eds.; Elsevier: Amsterdam, The Netherlands, 2019; pp. 1–26. [CrossRef]
3. Jadoun, S.; Arif, R.; Jangid, N.K.; Meena, R.K. Green synthesis of nanoparticles using plant extracts: A review. *Environ. Chem. Lett.* **2021**, *19*, 355–374. [CrossRef]
4. Shafey, A.M.E. Green synthesis of metal and metal oxide nanoparticles from plant leaf extracts and their applications: A review. *Green Process. Synth.* **2020**, *9*, 304–339. [CrossRef]
5. Singh, J.; Dutta, T.; Kim, K.-H.; Rawat, M.; Samddar, P.; Kumar, P. ‘Green’ synthesis of metals and their oxide nanoparticles: Applications for environmental remediation. *J. Nanobiotechnol.* **2018**, *16*, 84. [CrossRef]
6. Madkour, M.; Bumajdad, A.; Al-Sagheer, F. To what extent do polymeric stabilizers affect nanoparticles characteristics? *Adv. Colloid Interface Sci.* **2019**, *270*, 38–53. [CrossRef]
7. Tippayawat, P.; Phromviyo, N.; Boueroy, P.; Chompoosor, A. Green synthesis of silver nanoparticles in aloe vera plant extract prepared by a hydrothermal method and their synergistic antibacterial activity. *PeerJ* **2016**, *4*, e2589. [CrossRef]
8. Quispe, C.; Villalobos, M.; Bórquez, J.; Simirgiotis, M. Chemical composition and antioxidant activity of *Aloe vera* from the Pica Oasis (Tarapacá, Chile) by UHPLC-Q/Orbitrap/MS/MS. *J. Chem.* **2018**, *2018*, 6123850. [CrossRef]

9. Phang, Y.-K.; Aminuzzaman, M.; Akhtaruzzaman, M.; Muhammad, G.; Ogawa, S.; Watanabe, A.; Tey, L.-H. Green synthesis and characterization of CuO nanoparticles derived from papaya peel extract for the photocatalytic degradation of palm oil mill effluent (POME). *Sustainability* **2021**, *13*, 796. [[CrossRef](#)]
10. Hendra, R.; Masdeatresia, L.; Abdullah, R.; Haryani, Y. Red dragon peel (*Hylocereus polyrhizus*) as antioxidant source. *AIP Conf. Proc.* **2020**, *2243*, 030007. [[CrossRef](#)]
11. Manigandan, R.; Dhanasekaran, T.; Padmanaban, A.; Giribabu, K.; Suresh, R.; Narayanan, V. Bifunctional hexagonal Ni/NiO nanostructures: Influence of the core-shell phase on magnetism, electrochemical sensing of serotonin, and catalytic reduction of 4-nitrophenol. *Nanoscale Adv.* **2019**, *1*, 1531–1540. [[CrossRef](#)]
12. Sekar, S.; Kim, D.Y.; Lee, S. Excellent oxygen evolution reaction of activated carbon-anchored NiO nanotablets prepared by green routes. *Nanomaterials* **2020**, *10*, 1382. [[CrossRef](#)]
13. Munna, F.T.; Selvanathan, V.; Sobayel, K.; Muhammad, G.; Asim, N.; Amin, N.; Sopian, K.; Akhtaruzzaman, M. Diluted chemical bath deposition of CdZnS as prospective buffer layer in CIGS solar cell. *Ceram. Int.* **2021**, *47*, 11003–11009. [[CrossRef](#)]
14. Tripathi, R.M.; Bhadwal, A.S.; Gupta, R.K.; Singh, P.; Shrivastav, A.; Shrivastav, B.R. ZnO nanoflowers: Novel biogenic synthesis and enhanced photocatalytic activity. *J. Photochem. Photobiol. B Biol.* **2014**, *141*, 288–295. [[CrossRef](#)]
15. Lamba, P.; Singh, P.; Singh, P.; Kumar, A.; Singh, P.; Bharti, Kumar, Y.; Gupta, M. Bioinspired synthesis of nickel oxide nanoparticles as electrode material for supercapacitor applications. *Ionics* **2021**, *27*, 5263–5276. [[CrossRef](#)]
16. Cao, Y.; Hu, P.; Jia, D. Solvothermal synthesis, growth mechanism, and photoluminescence property of sub-micrometer PbS anisotropic structures. *Nanoscale Res. Lett.* **2012**, *7*, 668. [[CrossRef](#)]
17. Talluri, B.; Prasad, E.; Thomas, T. Ultra-small ($r < 2$ nm), stable (>1 year) copper oxide quantum dots with wide band gap. *Superlattices Microstruct.* **2018**, *113*, 600–607. [[CrossRef](#)]
18. Selvanathan, V.; Aminuzzaman, M.; Tey, L.-H.; Razali, S.A.; Alhubeiti, K.; Alkhamash, H.I.; Guha, S.K.; Ogawa, S.; Watanabe, A.; Shahiduzzaman, M.; et al. *Muntingia calabura* leaves mediated green synthesis of CuO nanorods: Exploiting phytochemicals for unique morphology. *Materials* **2021**, *14*, 6379. [[CrossRef](#)]
19. Liang, Q.; Brocks, G.; Bieberle-Hütter, A. Oxygen evolution reaction (OER) mechanism under alkaline and acidic conditions. *J. Phys. Energy* **2021**, *3*, 026001. [[CrossRef](#)]
20. Jin, H.; Wang, X.; Tang, C.; Vasileff, A.; Li, L.; Slattery, A.; Qiao, S.-Z. Stable and highly efficient hydrogen evolution from seawater enabled by an unsaturated nickel surface nitride. *Adv. Mater.* **2021**, *33*, 2007508. [[CrossRef](#)]
21. Wang, C.; Qi, L. Hollow nanosheet arrays assembled by ultrafine ruthenium-cobalt phosphide nanocrystals for exceptional pH-universal hydrogen evolution. *ACS Mater. Lett.* **2021**, *3*, 1695–1701. [[CrossRef](#)]
22. Rani, B.J.; Ravi, G.; Yuvakkumar, R.; Ravichandran, S.; Ameen, F.; Al-Sabri, A. Efficient, highly stable Zn-doped NiO nanocluster electrocatalysts for electrochemical water splitting applications. *J. Sol-Gel Sci. Technol.* **2019**, *89*, 500–510. [[CrossRef](#)]
23. Zhu, K.; Shi, F.; Zhu, X.; Yang, W. The roles of oxygen vacancies in electrocatalytic oxygen evolution reaction. *Nano Energy* **2020**, *73*, 104761. [[CrossRef](#)]
24. Wang, Y.; Liang, Z.; Zheng, H.; Cao, R. Recent progress on defect-rich transition metal oxides and their energy-related applications. *Chemistry* **2020**, *15*, 3717–3736. [[CrossRef](#)]
25. Wang, H.; Xie, A.; Li, X.; Wang, Q.; Zhang, W.; Zhu, Z.; Wei, J.; Chen, D.; Peng, Y.; Luo, S. Three-dimensional petal-like graphene Co₃O₄Cu₁ metal organic framework for oxygen evolution reaction. *J. Alloys Comp.* **2021**, *884*, 161144. [[CrossRef](#)]
26. Santos, H.L.S.; Corradini, P.G.; Medina, M.; Dias, J.A.; Mascaro, L.H. NiMo–NiCu Inexpensive Composite with High Activity for Hydrogen Evolution Reaction. *ACS Appl. Mater. Interfaces* **2020**, *12*, 17492–17501. [[CrossRef](#)]
27. Selvanathan, V.; Ruslan, M.H.; Aminuzzaman, M.; Muhammad, G.; Amin, N.; Sopian, K.; Akhtaruzzaman, M. Resorcinol-Formaldehyde (RF) as a Novel Plasticizer for Starch-Based Solid Biopolymer Electrolyte. *Polymers* **2020**, *12*, 2170. [[CrossRef](#)]
28. Akbayrak, M.; Önal, A.M. Metal oxides supported cobalt nanoparticles: Active electrocatalysts for oxygen evolution reaction. *Electrochim. Acta* **2021**, *393*, 139053. [[CrossRef](#)]